Optics Letters

All-polymer arrayed waveguide grating at 850 nm: design, fabrication, and characterization

Rozalia Orghici,[1,*] Konrad Bethmann,[2] Urs Zywietz,[3] Carsten Reinhardt,[3] and Wolfgang Schade[1,2]

[1]Clausthal University of Technology, Institute of Energy Research and Physical Technologies (IEPT) and Energy Research Center of Lower Saxony (EFZN), EnergieCampus, Am Stollen 19B, 38640 Goslar, Germany
[2]Fraunhofer Heinrich Hertz Institute, Department of Fiber Optical Sensor Systems, EnergieCampus, Am Stollen 19H, 38640 Goslar, Germany
[3]Laser Zentrum Hannover e.V., Hollerithallee 8, 30419 Hannover, Germany
*Corresponding author: rozalia.orghici@tu-clausthal.de

Received 26 May 2016; revised 1 August 2016; accepted 3 August 2016; posted 3 August 2016 (Doc. ID 267194); published 19 August 2016

In this Letter, a novel all-polymer arrayed waveguide grating (AWG) device with an operating wavelength around 850 nm is reported. The all-polymer AWG consists of polymer ridge waveguides fabricated on a thin poly(methyl methacrylate) foil via microscope projection photolithography. The developed device is suitable to be integrated into optical circuits, e.g., a planar polymer foil and, along with other optical integrated devices, to be used for different sensing applications. The functionality of the device is demonstrated by using a fiber Bragg grating sensor and performing strain measurements.

OCIS codes: (130.3120) Integrated optics devices; (160.5470) Polymers; (080.1238) Array waveguide devices; (060.3735) Fiber Bragg gratings.

http://dx.doi.org/10.1364/OL.41.003940

As a key component of the photonic integrated circuits, arrayed waveguide gratings (AWGs) are commonly used as wavelength multiplexers or demultiplexers in telecom applications. Various materials such as silica [1], silicon [2], silicon nitride [3,4], germanium [5], and different polymers [6–8] have been used for their fabrication, expanding in this way the application field of these devices from the visible to the middle-infrared spectral region. Besides their application as wavelength multiplexers or demultiplexers, the use of AWG devices for optical sensing [9] and as microspectrometers [2,10] has also been reported in the literature.

In recent years, the development of polymer-based optical devices has gained much attention because of the excellent potential of polymers to provide a new generation of cost-effective optical sensor systems for multiple applications. In addition, the availability of polymers with high optical properties promotes the development of such devices [11,12]. Over the past years, various polymer-based optical devices (e.g., microring resonators [13], Bragg grating filters [14], arrayed waveguide gratings [6,7], and Mach–Zehnder interferometers [15]) have been fabricated; however, most of them have been fabricated for applications in the spectral range around $\lambda = 1.55$ μm. As a fabrication technique for these devices, conventional or soft photolithography has been used. In addition, most of the developed polymer-based devices still use silicon as a carrier material.

The development of optical integrated devices in the near-infrared spectral region (700–1100 nm) has not yet been developed to such an extent as in the spectral range around $\lambda = 1.55$ μm, although this region is of particular interest for various sensing applications, especially due to the availability of low-cost light sources and detectors. In this spectral region, the development of a compact arrayed waveguide grating has been shown in the literature [4]. The developed AWG device, however, consists of silicon nitride and shows great performance in terms of optical loss, crosstalk, and small foot print. In this Letter, we report on the design, fabrication, and characterization of a novel all-polymer AWG with an operating wavelength around $\lambda = 850$ nm. We introduce a new material platform and a novel geometrical layout; we also demonstrate the functionality of the developed all-polymer AWG device in a readout system.

The all-polymer AWG consists of a single input waveguide, two free propagation zones (FPZs), a group of four arrayed waveguides, and two output waveguides. A schematic configuration and scanning electron microscope (SEM) view of the developed device is shown in Fig. 1. By designing the layout of the all-polymer AWG, we chose a geometry that is more favorable in terms of minimizing bend losses. Thus, in our design, straight arrayed waveguides were considered. To enable spatial separation of different wavelengths, we introduced a constant path length difference ΔL between the waveguides

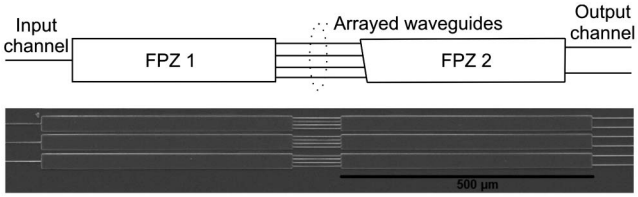

Fig. 1. Schematic configuration and SEM view of the AWG device.

in the array by modifying the second FPZ via inclination of the FPZ front.

The developed geometrical layout facilitates the integration of this optical device into an optical circuit, e.g., a planar polymer foil that contains further integrated devices (Bragg grating sensors, waveguide-based deformation sensors, etc.). Since many optical methods used in sensing applications require wavelength discrimination, the idea here is to use the developed all-polymer AWG as a spectrometer or an interrogator. Along with other integrated optical devices, the use of the presented device creates possibilities to set up new and cost-effective ways for optical measurement of different parameters, such as temperature, strain, pressure, or concentrations of molecular species in areas of medicine, life sciences, production technology, etc. In this Letter, we show a proof-of-principle concept for the measurement of strain by using a fiber Bragg grating (FBG) sensor and the developed all-polymer AWG.

The operation principle of an AWG, when used in the demultiplexing way, can be described as follows: light propagating in the input waveguide will be dispersed in the first FPZ and then coupled and individually guided into each waveguide of the array. The length of the arrayed waveguides is defined by the central wavelength of the AWG, i.e., the optical path length difference ΔL between adjacent waveguides equals an integer multiple of the central wavelength ($\Delta L = m\lambda_c/n_g$, with m being the order of the array, λ_c being the central wavelength, and n_g being the effective refractive index experienced by the waveguide mode). The output of the arrayed waveguides is dispersed again into a second FPZ, where each wavelength of the incoming light constructively interferes at a focal point at the output of the FPZ. Due to the constant path length difference between the waveguides in the array, each wavelength possesses a different phase front tilt, leading in this way to a dispersed spectrum at the end of the second FPZ. Spatial separation of the different wavelengths is obtained by placing waveguides at each of the focal points at the end of the second FPZ. A detailed description of the working principle of an AWG can be found in [16].

In a first step, extensive computational investigations were performed to determine both the geometrical dimensions of an all-polymer AWG and its spectral response. For the geometrical layout calculations, the fully vectorial mode solver tool FIMMWAVE (Photon Design) has been used. Here, limitations of the fabrication process (microscope projection photolithography [17]—MPP) were taken into account, i.e., a compromise between the total length of the AGW device (~2 mm) and the precision for the fabrication of narrow/single-mode waveguides had to be found. Simulations of the AWG spectral response were realized with the aid of the simulation tool BeamPROP (RSoft CAD Environment).

As a waveguide material, ormosil was chosen. This polymer possesses good optical properties and can easily be processed with MPP. Our AWG concept consists of ridge waveguides with air claddings which are to be fabricated on a flexible poly(methyl methacrylate) (PMMA) foil with a thickness of 120 ± 5 μm. The refractive indices of ormosil and PMMA foil at 850 nm are $n_{wg} = 1.52$ and $n_s = 1.49$, respectively.

In the computational investigations, waveguides with widths and heights of 2.5×1.5 μm, satisfying the single-mode condition, were considered. Furthermore, FPZs with widths and lengths of 30×500 μm were set, the front of the second

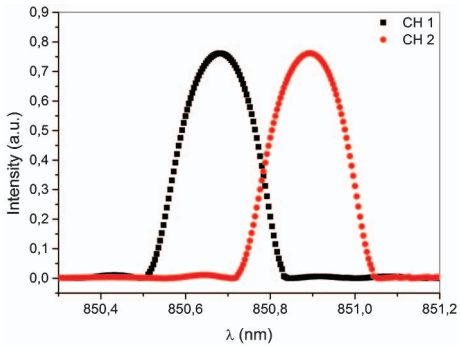

Fig. 2. Spectral transmission characteristics of an ideal all-polymer AWG device determined by the BeamPROP simulation tool.

FPZ inclined by 2.7°. The gap between the output channels was 18 μm. With these parameters, the spectral response of the all-polymer AWG device was determined. Resultant spectral transmission characteristics of the AWG as a function of the wavelength are shown in Fig. 2. The device with the parameters given above exhibits filter curves with a full width at half-maximum (FWHM) of about 190 pm and a channel spacing of about 220 pm. As can be seen, a spatial separation of the input light around $\lambda = 850$ nm can be obtained by using the AWG device with the novel straight waveguide configuration.

In a second step, the fabrication of the designed AWG device via MPP and its optical characterization has been realized. The PMMA foil has been covered with a layer of ormosil by spin-coating. A photomask containing the pattern defined with a chrome metal-absorbing film is placed into the light path of the microscope and projected through the microscope objective onto the PMMA-ormosil substrate. For illumination and initialization of the polymerization process, a high-power UV LED ($\lambda_{\mathrm{LED}} = 365$ nm, Roithner) was used. After washing of the sample with isopropanol, the cross-linked material forming the waveguides remains attached to the PMMA foil. A microscope view of the fabricated device can be seen in Fig. 1.

To characterize the fabricated AWG device, a fiber-coupled broadband superluminescent light emitting diode (SLED, Exalos) with a central wavelength of $\lambda_{\mathrm{SLED}} = 840$ nm, a FWHM of 50 nm, and an output power of $P = 3.5$ mW was used as the light source. Tapered lensed fibers (OZ Optics) were used to couple light into the input channel of the AWG and collect the light from the output channels. To measure the spectral response, the fiber situated at the output channel was connected to an optical spectrum analyzer (OSA, YOKOGAWA). In all computational investigations, the transverse electric (TE) polarization state was considered; however, experimentally we did not observe any polarization dependency for the developed device.

Figure 3(a) shows the spectral transmission characteristics of the fabricated all-polymer AWG device. For the fabricated device (SEM image in Fig. 1), filter curves with an FWHM of about 22 and 32 nm, respectively, and a spatial separation of 19 nm were obtained. The spectral broadening of the filter curves, as observed especially for the first output channel in Fig. 3(a), could be the result of inhomogeneities in the waveguide material or variations of the refractive index that arise during the UV curing process. In addition, an imperfect

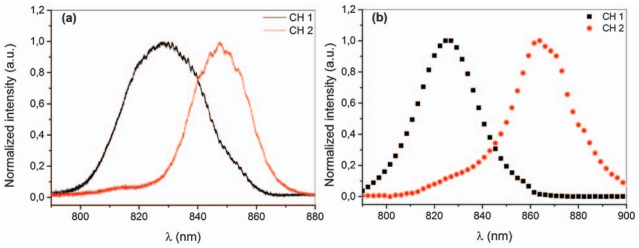

Fig. 3. (a) Measured spectral response of the fabricated all-polymer AWG. (b) Spectral response of the all-polymer AWG calculated with the parameters of the experimental AWG device.

fabrication of the device (slight variations of both the length of the arrayed waveguides and the lengths or widths of the FPZs) will influence the figure of merit of the initially designed AWG device. Therefore, in a next step, the dimensions of the fabricated AWG were determined via scanning electron microscopy. At this juncture, we observed that the dimensions of the manufactured AWG device indeed slightly differ from those considered in the computational investigations described above. The fabricated waveguides have widths and heights of 3.49 × 1.56 μm. The width of the output waveguides is 2.9 μm, and the gap between them is 16.19 μm. The width and length of the fabricated FPZs is 33.5 × 570 μm. The overall footprint of the device is about 0.035 × 1.7 mm.

With these parameters, a simulation of the transmission spectra was performed. Figure 3(b) depicts the calculated spectra via BeamPROP when broadband light is coupled into the device. It can be seen that a good agreement between the measured and calculated data can be obtained for the fabricated device. On closer examination of the calculated spectral response of the AWG [Fig. 3(b)], a redshift at the output of channel 2 was noted. This redshift, which amounts to 20 nm, could be caused by local variations of the refractive index of the waveguide material that may arise during the UV curing process. In addition, minor deviations from the stated lengths of the arrayed waveguides, which were extracted via SEM, or their inaccurate coupling to the second FPZ, will influence the channel spacing. All of these potential deviations were not included in the simulation, a fact that would explain the redshift at the output of channel 2, as observed for the simulated spectral response in Fig. 3(b).

The overall optical loss (loss due to coupling into and out of the waveguides, inhomogeneities in the waveguide material, surface roughness, crosstalk of channels, and imperfect fabrication) for the designed AWG is about −31 dB. Both the optical loss and the differences between designed and experimentally recorded spectral response of the AWG device can be further improved by optimizing the fabrication process (MPP), this being part of our current investigations.

Furthermore, a proof-of-principle investigation was conducted on the suitability of the fabricated AWG device for being integrated with other optical devices (e.g., a FBG sensor) and used, for instance, for strain measurements. The idea here is to use the AWG device for the readout of the FBG sensor when strain is applied to the fiber and, accordingly, a wavelength shift of the sensing FBG is induced. If the FBG reflection overlaps the spectral profile of the AWG output channel, the strain-induced wavelength shift can be converted into the

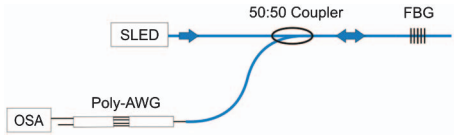

Fig. 4. Schematic configuration of the experimental setup for the FBG strain measurement with the all-polymer AWG.

measurement of an intensity change. Here, the intensity will be measured by attaching a photodiode array to the output channels of the AWG device. In this way, a compact and cost-effective readout unit can be built. This concept has already been shown in the literature for some applications that use silicon-based AWGs in the spectral range around $\lambda = 1.55$ μm [18,19].

In this Letter, the functionality of the developed all-polymer AWG device for the readout of a FBG sensor is demonstrated by considering the spectral profile of channel 2 that is displayed in Fig. 3(a). For this investigation, a Bragg grating with the central wavelength $\lambda_{FBG} = 843.2$ nm was inscribed into the core of a single-mode glass fiber by using the point-by-point technique with femtosecond laser pulses. The experimental setup and the inscription process are described in [20]. The FBG works in the reflection mode; it has a length of 1.8 mm and a FWHM of 0.26 nm. The central wavelength of the FBG overlaps the filter curve of the AWG device on its short wavelength edge.

Figure 4 depicts the experimental setup used for this investigation. The FBG sensor is illuminated by the SLED using a 50:50 coupler (Thorlabs). The reflected FBG signal is coupled into the AWG device, whereas the signal at the output of the AWG is analyzed with the OSA. When a strain is applied to the FBG sensor, both a redshift and an intensity change of the FBG signal are measured. Figure 5(a) shows the measured FBG reflection spectra for three different strains. The FBG peak intensities, which are displayed in Fig. 5(b), were extracted

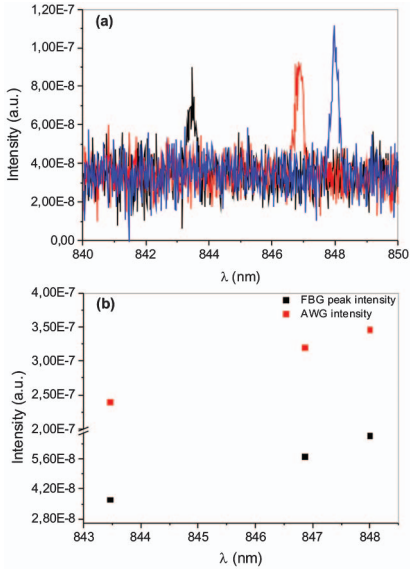

Fig. 5. Strain measurement. (a) FBG reflection spectra for different strains. (b) AWG and FBG peak intensities.

from the strain measurement by applying a Gaussian fit to each strain-induced FBG reflection spectrum. For comparison, intensities extracted from the measured filter curve of the AWG, which correspond to each strain-induced Bragg wavelength, were plotted in Fig. 5(b). As expected for the steep slope, it can be seen that the intensity of the FBG reflection increases with increasing of the strain, showing a good agreement with the increased intensity of the AWG filter curve. If the central wavelength of the FBG would be set on the falling slope, a decrease in the FBG peak intensity would be measured. Furthermore, the intensity change of the FBG signal due to the applied strain on the FBG sensor can be calibrated so that an exact value of the strain can be determined.

In this Letter, the development of a novel all-polymer AWG device with an operation wavelength around $\lambda = 850$ nm has been presented. Computational investigations were performed to identify an appropriate geometrical layout that allows the fabrication of the device on a thin polymer foil (PMMA). With the new design, an all-polymer AWG was fabricated via MPP. Experimental measurements attest computational investigations showing that a spatial wavelength separation can be achieved by using the developed device with the novel straight waveguide configuration. As a proof-of-concept, the suitability of the AWG for the readout of an FBG sensor was successfully demonstrated by performing strain measurements.

Even if the developed AWG device does not yet excel in terms of spectral broadening and optical loss, as is common for devices fabricated via conventional UV photolithography, it shows tremendous potential to be used in multiple sensing applications due to the materials involved, the operating wavelength, and the straight waveguide configuration. In addition, MPP as a fabrication technique enables sensor networks to be easily manufactured on different spots of the polymer foil on a very fast timescale. Depending on the application, cost-effective and customized AWGs could be fabricated with this technique.

Current investigations focus on studying the thermal behavior of the fabricated device and achieving its athermal behavior. In addition, the use of other polymers with different thermo-optic coefficients is envisaged.

Funding. Deutsche Forschungsgemeinschaft (DFG) (SFB/TRR 123).

REFERENCES

1. T. Saida, A. Kaneko, T. Goh, M. Okuno, A. Himeno, K. Takiguchi, and K. Okamoto, Electron. Lett. **36**, 528 (2000).
2. P. Cheben, J. H. Schmid, A. Delage, A. Densmore, S. Janz, B. Lamontagne, J. Lapointe, E. Post, P. Waldron, and D. X. Xu, Opt. Express **15**, 2299 (2007).
3. D. X. Dai, Z. Wang, J. F. Bauters, M. C. Tien, M. J. R. Heck, D. J. Blumenthal, and J. E. Bowers, Opt. Express **19**, 14130 (2011).
4. D. Martens, A. Z. Subramanian, S. Pathak, M. Vanslembrouck, P. Bienstman, W. Bogaerts, and R. G. Baets, IEEE Photonics Technol. **27**, 137 (2015).
5. A. Malik, M. Muneeb, S. Pathak, Y. Shimura, J. Van Campenhout, R. Loo, and G. Roelkens, IEEE Photonics Technol. **25**, 1805 (2013).
6. N. Keil, H. H. Yao, C. Zawadzki, J. Bauer, M. Bauer, C. Dreyer, and J. Schneider, Electron. Lett. **37**, 579 (2001).
7. B. Yang, Y. P. Zhu, Y. Q. Jiao, L. Yang, Z. Sheng, S. L. He, and D. X. Dai, J. Lightwave Technol. **29**, 2009 (2011).
8. J. S. Kee, D. P. Poenar, P. Neuzil, L. Yobas, and Y. Chen, Opt. Express **18**, 21732 (2010).
9. K. Kodate and Y. Komai, J. Opt. A **10**, 044011 (2008).
10. Z. X. Hu, A. Glidle, C. Ironside, J. M. Cooper, and H. B. Yin, Lab Chip **15**, 283 (2015).
11. L. Eldada, Proc. SPIE **5931**, 59310F (2005).
12. M. C. Oh, K. J. Kim, W. S. Chu, J. W. Kim, J. K. Seo, Y. O. Noh, and H. J. Lee, Polymers **3**, 975 (2011).
13. Y. Y. Huang, G. T. Paloczi, J. K. S. Poon, and A. Yariv, Appl. Phys. Lett. **85**, 3005 (2004).
14. D. H. Kim, W. J. Chin, S. S. Lee, S. W. Ahn, and K. D. Lee, Appl. Phys. Lett. **88**, 071120 (2006).
15. G. T. Paloczi, Y. Y. Huang, A. Yariv, and S. Mookherjea, Opt. Express **11**, 2666 (2003).
16. M. K. Smit and C. vanDam, IEEE J. Sel. Top. Quantum Electron. **2**, 236 (1996).
17. J. C. Love, D. B. Wolfe, H. O. Jacobs, and G. M. Whitesides, Langmuir **17**, 6005 (2001).
18. Y. Sano and T. Yoshino, J. Lightwave Technol. **21**, 132 (2003).
19. J. Koch, M. Angelmahr, and W. Schade, Appl. Opt. **51**, 7718 (2012).
20. C. Waltermann, J. Koch, M. Angelmahr, J. Burgmeier, M. Thiel, and W. Schade, *Planar Waveguides and Other Confined Geometries: Theory, Technology, Production, and Novel Applications*, G. Marowsky, ed. (Springer, 2015), pp. 227–250.